Ideal, constant-loss nanophotonic mode converter using a Lagrangian approach

Alexandre Horth,[1,5] **Pavel Cheben,**[2] **Jens H. Schmid,**[2] **Raman Kashyap,**[3] **and Nathaniel J. Quitoriano**[4,6]

[1]*Department of Electrical and Computer Engineering, McGill University, Canada*
[2]*Information and Communications Technologies Portfolio, National Research Council Canada, Ottawa ON K1A 0R6, Canada*

[3]*Department of Engineering Physics and Department of Electrical Engineering, Ecole Polytechnique de Montreal, Montreal QC H3C 3A7, Canada*

[4]*Department of Mining and Materials Engineering, McGill University, 3610 University Street #2620, Montreal QC H3A 2B2, Canada*

[5]*alexandre.horth@mail.mcgill.ca*
[6]*nate.quitoriano@mcgill.ca*

Abstract: Coupling light between an optical fiber and a silicon nanophotonic waveguide is a challenge facing the field of silicon photonics to which various mode converters have been proposed. Inverted tapers stand out as a practical solution enabling efficient and broadband mode conversion. Current design approaches often use linearly-shaped tapers and two dimensional approximations; however, these approaches have not been rigorously verified and there is not an overarching design framework to guide the design process. Here, using a Lagrangian formulation, we propose an original, constant-loss framework for designing shape-controlled photonic devices and apply this formalism to derive an ideal constant-loss taper (CLT). We specifically report on the experimental demonstration of a fabrication-tolerant, 15-μm-long CLT coupler, that produces 0.56 dB fiber-chip coupling efficiency, the highest efficiency-per-length ratio ever reported.

OCIS codes: (130.0130) Integrated optics; (250.0250) Optoelectronics; (130.3120) Integrated optics devices.

References and links

1. R. Soref, "The past, present, and future of silicon photonics," IEEE J. Sel. Top. Quantum Electron. **12**(6), 1678–1687 (2006).
2. A. Rickman, "The commercialization of silicon photonics," Nat. Photonics **8**, 579–582 (2014).
3. Y. A. Vlasov, and S. J. McNab, "Losses in single-mode silicon-on-insulator strip waveguides and bends," Opt. Express **12**(8), 1622–1631 (2004).
4. M. M. Spuhler, B.J. Offrein, G-L. Bona, and R. Germann, "A very short planar silica spot-size converter using a nonperiodic segmented waveguide," J. Lightwave Technol. **16**(9), 1680–1685 (1998).
5. D. Taillaert, F. Van Laere, M. Ayre, and W. Bogaert, "Grating couplers for coupling between optical fibers and nanophotonic waveguides," Jpn. J. Appl. Phys. **45**(1-8A), 6071–6077 (2006).
6. B. Shen, P. Wang, R. Polson, and R. Menon, "An integrated-nanophotonics polarization beamsplitter with 2.4um2 footprint," Nat. Photonics **9**(6), 378–382 (2015).
7. M. Pu, L. Liu, H. Ou, K. Yvind, and J. M. Hvam, "Ultra-low-loss inverted taper coupler for silicon-on-insulator ridge waveguide," Opt. Commun. **283**(19), 3678–3682 (2010).
8. P. Cheben, P. J. Bock, J. H. Schmid, J. Lapointe, S. Janz, D.-X. Xu, A. Densmore, A. Delage, B. Lamontagne, and T. J. Hall, "Refractive index engineering with subwavelength gratings for efficient microphotonic couplers and planar waveguide multiplexers," Opt. Lett. **35**(15), 2526–2528 (2010).

#255259 Received 25 Jan 2016; revised 5 Mar 2016; accepted 9 Mar 2016; published 17 Mar 2016

9. P. Cheben, J. H. Schmid, S. Wang, D.-X. Xu, M. Vachon, S. Janz, J. Lapointe, Y. Painchaud, and M.-J. Picard, "Broadband polarization independent nanophotonic coupler for silicon waveguides with ultra-high efficiency," Opt. Express **23**(17), 22553 (2015).
10. T. Shoji, T. Tsuchizawa, T. Watanabe, K. Yamada and H. Morita, "Low loss mode size converter from 0.3 mu m square si wire waveguides to singlemode fibres," Electron. Lett. **38**(25), 1669–1670 (2002).
11. V. R. Almeida, R. R. Panepucci, and M. Lipson, "Nanotaper for compact mode conversion," Opt. Lett. **28**(15), 1302–1304 (2003).
12. S.J. McNab, N. Moll, and Y. A. Vlasov, "Ultra-low loss photonic integrated circuit with membrane-type photonic crystal waveguides," Opt. Express **11**(22), 2927–2939 (2003).
13. I.D. Rukhlenko, M. Premaratne and G. P. Agrawal, "Effective mode area and its optimization in silicon-nanocrystal waveguides," Opt. Lett. **37**(12), 2295–2297 (2012).
14. Y. Fu, T. Ye, W. Tang and T. Chu "Efficient adiabatic silicon-on-insulator waveguide taper," Photon. Res. **2**(3), A41–A44 (2014).
15. X. Xu, H. Subbaraman, J. Covey, D. Kwong, A. Hosseini, and R. T. Chen, "Complementary metal–oxide–semiconductor compatible high efficiency subwavelength grating couplers for silicon integrated photonics," Appl. Phys. Lett. **101**(3), 031109 (2012).
16. E.-G. Newmann, *Single-Mode Fibers* (Springer, 1988).
17. J. T. Robinson, K. Preston, O. Painter, and M. Lipson, "First-principle derivation of gain in high-index-contrast waveguides," Opt. Express **16**(21), 16659–16669 (2008).
18. E. Butkov, *Mathematical Physics* (Addison Wesley, 1968).
19. D. Marcuse, "Radiation losses of tapered dielectric slab waveguides," Opt. Express **49**(2), 279–290 (1970).
20. D. L. Lee, *Electromagnetic Principles of Integrated Optics* (Wiley, 1986).
21. F. Grillot, L. Vivien, S. Laval, D. Pascal, and E. Cassan, "Size influence on the propagation loss induced by sidewall roughness in ultrasmall SOI waveguides," IEEE Photonics Technol. Lett. **16**(7), 1661–1663 (2004)

1. Introduction

The large index of refraction contrast of a silicon-on-insulator (SOI) platform enables high-density, cost-effective photonics on a chip. [1, 2] The typical interconnecting channel waveguide on 220 nm SOI has a 450 nm width resulting in a tightly confined mode profile. This type of waveguide is often used to connect integrated devices together since it minimizes the mode area of the waveguide, thereby enabling high-density optical circuitry while keeping the propagation loss small over short distances. [3] However, at the junction between the interconnecting waveguide and the chip external coupling interface there is an intrinsic mode mismatch requiring mode conversion. [4–12] Tapers are used to gradually convert the mode area and the effective index of the guided mode, typically by varying the waveguide width. In Fig. 1(a), the effective mode area (EMA) of a 220 nm thick SOI waveguide is shown as a function of the waveguide width (w) using a full-vectorial mode solver (FULL, solid line) at $\lambda = 1550$ nm. The top-left inset shows the waveguide geometry with the main regions of interest: core, side, and corner. It is observed that the EMA is minimized for the single-mode condition at point (c) ($w = 450$ nm, Fig. 1(a)). Here, the EMA is defined as: [13]

$$EMA = \left(\iint S_z dxdy \right)^2 \Big/ \iint S_z^2 dxdy \tag{1}$$

where $S_z = (\mathbf{E} \times \mathbf{H}) \cdot \hat{z}$ is the Poynting vector, $\hat{z}$ is the unitary vector along the waveguide's propagation axis. Between points (c)→(d), the EMA undergoes a direct, linear expansion as shown in the bottom inset of Fig. 1(a). During this process, the guided mode remains primarily confined in the silicon core (Fig. 1(c) and 1(d); FULL) since its effective index remains substantially larger than the cladding index, $n_{clad} \sim 1.46$. Because of this core-confined mode profile, the mode area can be well approximated by the dimensions of the core itself, *i.e.* $EMA \cong w \times h$, where h is the waveguide thickness and w is the waveguide width; thus explaining the linear mode expansion relationship. As a result of this linear behaviour, tapers used for a direct expansion almost exclusively use a linear tapering shape, other shapes have been considered showing only marginal improvements. [14] Furthermore, from the evaluated mode profiles (Fig. 1(c)

#255259 Received 25 Jan 2016; revised 5 Mar 2016; accepted 9 Mar 2016; published 17 Mar 2016

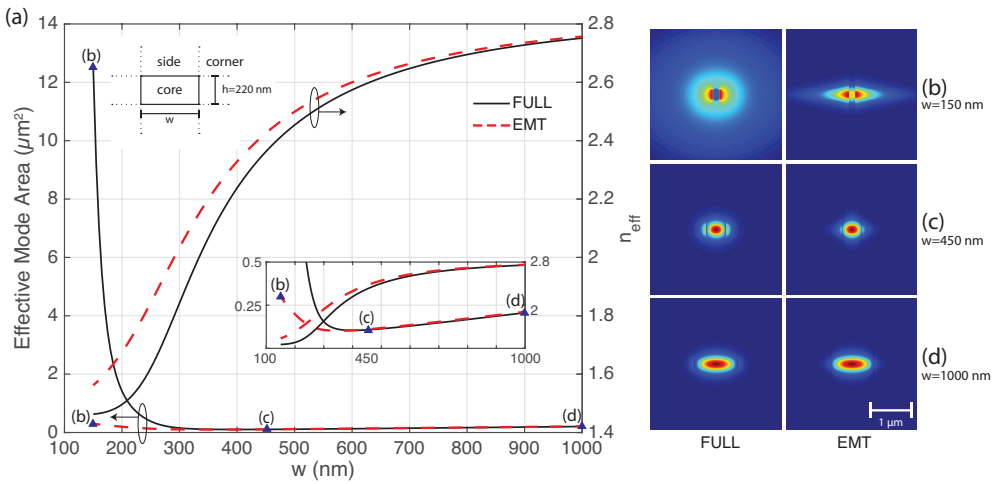

Fig. 1. In (a), the effective mode area and effective index (n_{eff}) of the fundamental quasi-TE mode is plotted for $\lambda = 1550$ nm for varying waveguide core width a core thickness of 220 nm. The solid line shows the results calculated using a full-vectorial (FULL) mode solver while the dashed line corresponds to the effective medium theory (EMT). Top-left inset shows the cross-section of the waveguide, bottom inset shows a close-up of the effective mode area as a function of waveguide width. The major component of the electric field of the guided mode is shown at three points on interest: w =150 nm, (b); 450 nm, (c); and 1000 nm, (d).

and 1(d); FULL) it can be seen that the amount of power located in the corner regions of the waveguide is negligible. This allows the use of the effective medium theory (EMT), which separates the field of the guided mode into Cartesian coordinates: $\psi = \psi_x \psi_y$. Using the EMT simplifies the structure to two simple one-dimensional slabs and reduces three-dimensional finite-difference time-domain (FDTD) simulations to a less computational intensive 2.5D FDTD. In Fig. 1(a), the EMT approximation (broken line) is applied in the direct expansion regime, with the calculated effective indices and mode profiles well approximated by the effective medium theory (Fig. 1(c) and 1(d); FULL vs EMT), thus confirming the validity of the approximation in this region.

From point (c) of Fig. 1(a) the mode area can also be increased through an indirect expansion by reducing the width of the waveguide. As w is reduced and reaches subwavelength dimensions, $< \lambda/2n$, the guided mode can no longer be tightly localized. As a result, the effective index of the waveguide abruptly drops, approaching that of the cladding material, leading to a strong, non-linear expansion of the mode area as seen in the (c)→(b) region. This mode expansion mechanism is often used to design nanophotonic mode converters for fiber-chip coupling. [7, 8, 10, 11] However, the EMT can no longer be applied in this subwavelength regime since the amount of power in the waveguide corner regions exceeds 80%, as seen at w = 150 nm in Fig. 1(b); FULL vs EMT. Although the EMT has been used in the inverse expansion regime [11, 15], its use seriously compromises the results. Here, using a full vectorial solver, an inverse taper is designed for maximum coupling efficiency between a 4.9 μm mode-field diameter (MFD) fiber and a silicon waveguide (450 nm $\times$ 220 nm) for TE polarized light at $\lambda = 1550$ nm.

#255259 Received 25 Jan 2016; revised 5 Mar 2016; accepted 9 Mar 2016; published 17 Mar 2016

2. Taper tip optimization

The coupling efficiency between an optical fiber and a SOI waveguide is determined by two main factors: the overlap integral of the electromagnetic fields between the fiber and the SOI waveguide at the tip of the taper, and the efficiency of the mode conversion process between the taper tip and the interconnecting waveguide. Figure 2. shows the overlap integral between an optical fiber (MFD=4.9 μm; E_i, H_i) and a silicon waveguide of different widths (E_j, H_j). The overlap integral, η, is defined as: [16]

$$\eta = \frac{\left| \iint E_i \times H_j^* dxdy \right|^2}{\left| \iint E_i \times H_i^* dxdy \right| \cdot \left| \iint E_j \times H_j^* dxdy \right|} . \tag{2}$$

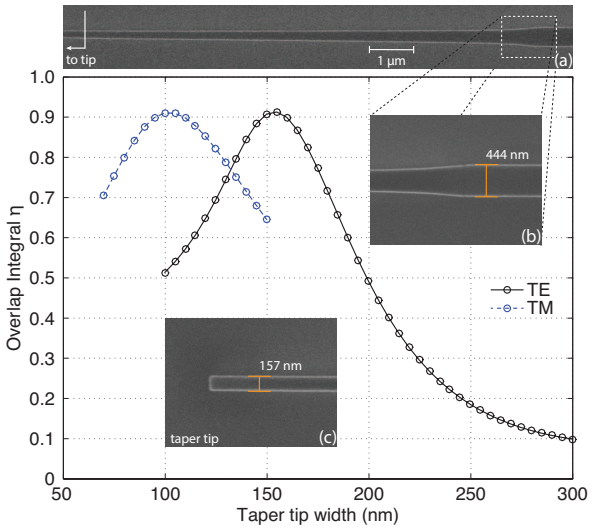

Fig. 2. The overlap integral between the modes of a 4.9 μm MFD fiber and the taper tip of varying widths for quasi-TE and -TM polarization. (a) Fabricated 15-μm-long constant-loss taper optimized for TE coupling, (b) distinctive feature of the constant-loss taper (CLT) that abruptly expands near the final 450 nm width, and (c) the taper tip.

The overlap integral is maximized for w_0 of 155 nm and 100 nm at $\eta = 0.92$ (0.36 dB) for the quasi-TE and -TM modes, respectively. The overlap integral sets the upper limit of coupling efficiency since additional loss is expected as the mode propagates through the taper. In the calculation of the overlap integral, the magnetic field should not be simplified as a direct function of its electric counterpart because the SOI waveguide modes are not well approximated by propagating plane waves; they are quasi-TE/TM modes. [17] Accounting for the magnetic components of the guided modes leads to the calculation of optimal tip widths that are 20-30 nm larger than those previously reported [11].

3. Constant-loss framework

Now that the overlap integral is maximized at the taper's tip, the tapering function needs to be optimized for maximum light coupling efficiency between the tip and the interconnecting waveguide. The range of different, monotonically increasing taper functions to connect the taper tip (width, w_0) to the waveguide (width, w_{out}) in a given taper length, L, is bounded by the two

#255259 Received 25 Jan 2016; revised 5 Mar 2016; accepted 9 Mar 2016; published 17 Mar 2016

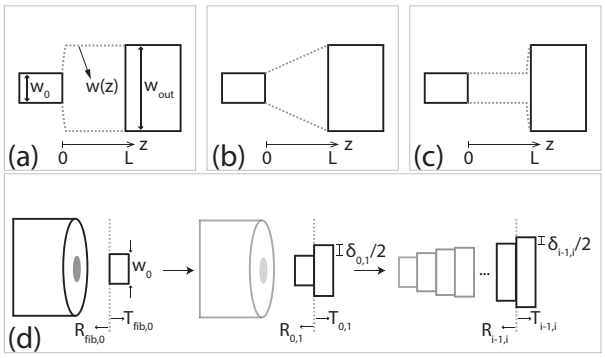

Fig. 3. Top three pictograms show various monotonically increasing tapering functions. (a) and (c) present the limit cases of potential taper functions; (b) presents an example of a taper function, the linear taper. (d) presents a method of deriving the constant-loss taper; at step *0* the taper tip is defined by maximizing the overlap intergral with the fiber, in step *1* a waveguide step, δz_1, is selected that produces a constant mode mismatch loss, $\alpha_{threshold}$. Recursively, the following *ith* steps can be defined by selection a waveguide step $\delta z_{i-1,i}$ leading to $\alpha_{i-1,i} = \alpha_{threshold}$.

taper functions shown in Fig. 3(a) and 3(c). These piecewise functions are equivalent to each other, under the assumption that untapered waveguides are lossless. Given that these functions are abrupt, they represent the least efficient taper functions possible. In-between these cases an optimal taper function, that maximizes the efficiency can be inferred. Among the possible taper functions, the linear taper (Fig. 3(b)) or the parabolic functions are often used [10, 11], because of their simplicity but not necessarily optimal efficiency. To determine a taper shape with the highest possible efficiency, let us first define the total loss, $L\{w\}$, incurred by a taper function, $w(z)$ and the instantaneous taper loss at point z as $\alpha(w, \dot{w}, z)$. The total loss of the taper can be expressed by the following functional:

$$L\{w\} = \int_0^L \alpha\,(w, \dot{w}, z)\, dz\ . \tag{3}$$

The optimal taper function $w(z)$ that minimizes $L\{w\}$ can be derived by solving the Euler-Lagrange differential equation: [18]

$$\frac{\partial \alpha}{\partial w} - \frac{d}{dz}\left(\frac{\partial \alpha}{\partial \dot{w}}\right) = 0\ . \tag{4}$$

Assuming that α does not depend explicitly on z, which is a reasonable hypothesis under the assumption that an untapered waveguide is lossless and that $w(z)$ is a monotonically varying function, the following simplified equation is obtained:

$$\alpha = \dot{w}\frac{\partial \alpha}{\partial \dot{w}} = \text{cst.} \tag{5}$$

This implicit equation provides a clear guideline for designing an optimal taper function: the instantaneous loss at any point z within $w(z)$ should be constant. Equation 5 establishes a general design principle that can be applied to engineer different types of photonic devices with varying shape functions. For an inverse taper, $\alpha(w, \dot{w})$ depends on the coupling between the guided mode and the radiation modes. Given the infinite number of radiation modes, this

#255259 Received 25 Jan 2016; revised 5 Mar 2016; accepted 9 Mar 2016; published 17 Mar 2016

calculation is computationally intensive. However, because at any point z along the taper only a single guided mode is supported, the instantaneous transmitted (T) and reflected (R) powers between the guided modes at $z-$ and $z+$ can be tracked. This approach is complementary to computing the instantaneous power loss to the radiation modes, *i.e.* $\alpha = 1 - R - T$. Figure 3(d) schematically shows our taper design approach where the taper function is discretized into steps. The width of the first step, w_0, is selected to maximize the overlap integral with the optical fiber mode (Fig. 2.); then, recursively, the taper is constructed by adding steps widths, $\delta_{i-1,i} = |w_{i-1} - w_i|$, selected such that the loss penalty is constant, $\alpha_{i-1,i} = \alpha_{threshold}$. To compute the step loss, a coupled-mode theory is employed, leading to the following equations: [19, 20]

$$\begin{aligned} T_{i-1,i} &= \eta_{i-1,i} \\ R_{i-1,i} &= \left| \frac{n_{eff_{i-1}} - n_{eff_i}}{n_{eff_{i-1}} + n_{eff_i}} \right|^2 \\ \alpha_{i-1,i} &= (1 - R - T) \cong (1 - T) = \alpha_{threshold} = \text{cst.} \end{aligned} \tag{6}$$

In practice, the reflection coefficient is several orders of magnitude smaller than the transmission coefficient and can often be neglected.

4. Results

4.1. Power tracking

Figure 4(a) compares the width of three different, 15-μm-long taper functions: linear, parabolic, and constant-loss, as calculated using the methodology presented in the previous section. Figure 4(b) shows the power in the guided mode using a 3D FDTD simulation.

In Fig. 4(b), at a given position z, the total power (P_z) is compared to the gaussian, 4.9 μm MFD source power, $\Gamma_{z,source} = P_z / P_{source}$. Subsequently, the overlap integral between the field distribution and the local guided mode at z is calculated to obtain the power in the guided mode, $P_{mode}(z) = \Gamma_{z,source} \cdot \eta_{z,mode}$. In Fig. 4(b), all three tapers start with 92% of the source power guided in the tip mode (Fig. 2). In the linear taper, light is substantially dissipated near the tip as the mode propagates along the first 4 μm of the taper. The parabolic taper, whose width increases more slowly initially, yields an improved taper function. The best taper function is the constant-loss taper in which the mode conversion loss is more evenly distributed along the taper, in spite of the fast tapering rate in the 13-15 μm range (Fig. 4(a)). The not quite linear power decay characteristic of the CLT in Fig. 4(b) is likely because a simple coupled-mode theory formalism was used to implement the constant-loss formalism; use of a finer 3D FDTD mesh could also improve the linearity of the loss profile. Halfway through the taper, the electric fields along the constant-loss taper and linear taper are compared in Fig. 4(d) and 4(e), respectively. In this region, the constant-loss taper is in an intermediate state of field delocalization while the mode conversion process of a linear taper is mostly completed, indicating that the constant-loss taper shape more efficiently uses the conversion length L available.

4.2. Taper length dependency

Figure 5 shows the coupler efficiency as a function of taper length simulated in 3D FDTD. One can observe that the efficiency of the couplers increases with increasing taper lengths; furthermore, the CLT is found to be more efficient than either the parabolic or linear taper shape, for any taper length. It is worth nothing that the simulations that were used to compute the curves in Fig. 5 did not include a finite buried oxide layer (BOX) and therefore radiation losses to the substrate are neglected; *i.e.* Fig. 5 shows how the coupler efficiency is impacted by the mode transformation loss only. In actuality, radiation losses to the substrate would limit the maximal

#255259 Received 25 Jan 2016; revised 5 Mar 2016; accepted 9 Mar 2016; published 17 Mar 2016

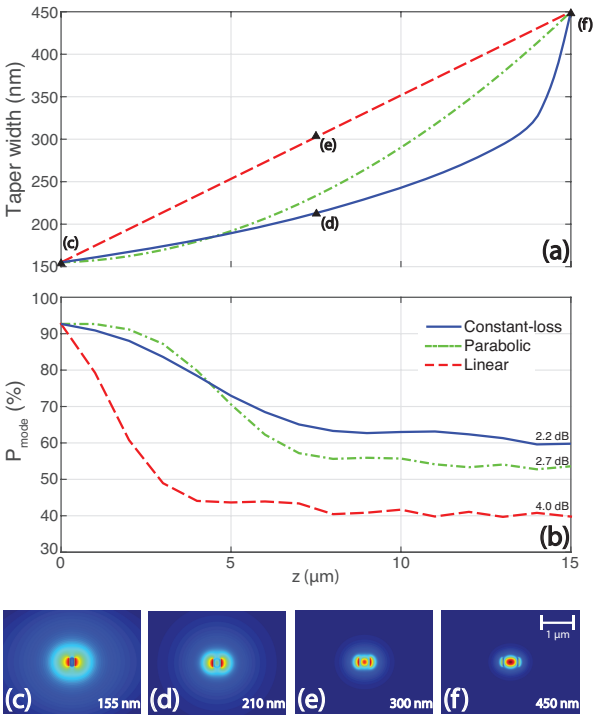

Fig. 4. (a) The width of the linear, parabolic and constant-loss taper as calculated using the constant-loss methodology. (b) The power in the guided mode (P_{mode}) at a position z within the taper is tracked for the various taper functions. The bottom figures (c)–(f) show the major component of the electric field at 4 different positions; (c) and (f) show the input (155 nm) and output (450 nm) modes.

achievable efficiency; as the tapers are made longer, the gain in efficiency that a smoother mode transformation process brings diminishes, as seen in Fig. 5 at longer taper length, while the radiative losses would steadily increase with length. For example, a 15-μm-long constant-loss taper has approximately the same efficiency mode transformation loss than a 22-μm; but the parabolic taper, being longer, would suffer from greater radiation losses. An important goal in designing practical edge coupling structures is to expand the mode size to match fibers with large mode field diameters in order to relax the fiber alignment tolerances. For typical BOX layer thicknesses used (2-3 μm) loss by light leaking into the substrate becomes a limiting factor to the overall coupling efficiency. These substrate losses can be minimized for a given mode size by minimizing the taper length, the constant-loss taper quantifies the miniaturization that can be achieved by optimal design of the widely used inverse taper couplers.

4.3. Taper robustness to fabrication

In Figure 5, the linear (and to a lesser extent the parabolic) taper exhibits a pronounced point-to-point jaggedness (four points are specifically shown). This is attributed to the 3D FDTD grid approximating the taper. Because the CLT's shape is close to minimizing the coupler's loss at each point, shape distortions incurred by the mesh affect less its efficiency compared to the linear shape. The mesh distortions effect is roughly analogous to the distortions that can be introduce in fabrication; therefore the CLT is expected to be more robust to fabrication.

In order to further demonstrate the robustness of the constant-loss taper to fabrication, 15-

#255259 Received 25 Jan 2016; revised 5 Mar 2016; accepted 9 Mar 2016; published 17 Mar 2016

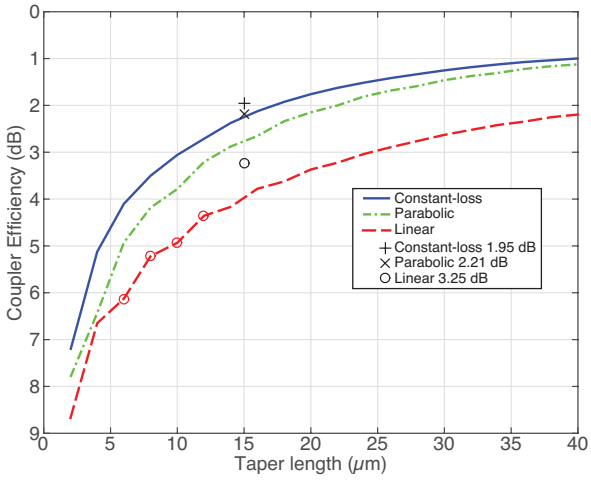

Fig. 5. Coupler efficiency as a function of the taper length with a 4.9 μm MFD fiber using a 3D FDTD simulation and measured efficiency for 15 μm long tapers.

μm-long tapers were perturbed using an exponential autocorrelation roughness model [21] with a standard deviation of 25 nm and a autocorrelation length of 250 nm. A total of 100 perturbation profiles were generated for each coupler and then simulated in 3D FDTD. Figure 6 reports the normalized probability distribution of the coupler efficiency given our perturbation model. It can clearly be seen that not only is the constant-loss taper more efficient, but its distribution is more tightly grouped near the unperturbed taper's efficiency showing that the constant-loss taper is indeed more robust to fabrication than the linear or parabolic liner taper. The linear taper actually has some perturbed tapers (5 counts) that outperformed the unperturbed case; the efficiency of the linear taper is very sensitive to perturbation that occurs near its tip, as seen in Fig. 4(b), as a result perturbations that resulted in making the tip of the linear taper less abrupt resulted in a slightly better coupler. The median coupler efficiency are 5.0, 4.6, and 3.5 dB; respectively for a linear, parabolic, and constant-loss taper. In an industrial setting, producing components that have increased robustness to fabrication is key in improving one's fabrication yield, use of a constant-loss taper would result in improved taper fabrication robustness.

4.4. Experimental results

Inverted tapers were fabricated using a 220 nm silicon-on-insulator wafer with 3 μm buried oxide layer. The structures were defined using a hydrogen silsesquioxane (HSQ) resist with a inductively coupled, $SF_6 - C_4F_8$ plasma etching and covered in a 3 μm thick plasma enhanced chemical vapor deposition (PECVD) oxide. In Fig. 5, at a $\sim$ 15 μm taper length, the expected efficiency of a constant-loss taper is noticeably higher compared to a linear or parabolic taper, therefore 15 μm long tapers were fabricated. Using a tunable laser and a polarization controller, light was coupled to a polarization-maintaining, 5 μm MFD or 3 μm MFD, lens fiber. The insertion loss of a single coupler was determined by measuring the total insertion loss to the chip, the total loss is composed of the loss from the input coupler, the waveguide, and the output coupler. The loss from the waveguide was de-embed from the the total insertion by measuring the waveguide loss through the cut-back method. Specifically, the waveguide loss was measure at 1.1 dB/cm or 0.53 dB for our 4800 μm long waveguide. This low waveguide loss enables precise measurement of the coupler's loss given that only 0.53 dB had to be deducted from the total insertion loss measurement in order to receive the couplers' loss.

#255259 Received 25 Jan 2016; revised 5 Mar 2016; accepted 9 Mar 2016; published 17 Mar 2016

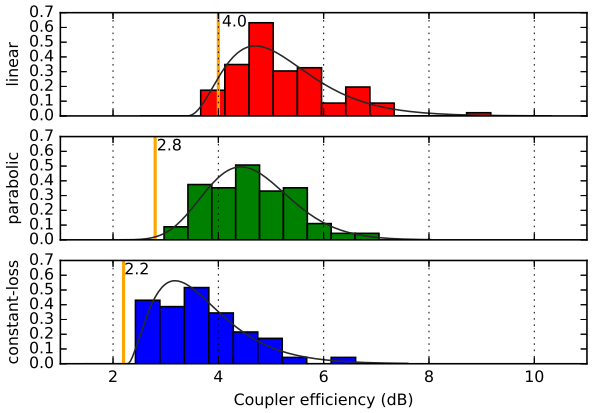

Fig. 6. Distribution of the coupler loss efficiency given roughness perturbations for a linear, parabolic, and constant-loss taper; the median coupler efficiency are 5.0, 4.6, and 3.5 dB, respectively. Vertical annotatted line show the reference coupler efficiency of an unperturbed taper.

The measured efficiencies are reported in Fig. 5 for the 5 μm MFD fiber. The CLT is the best taper at 1.95 dB followed the parabolic, 2.21 dB, and linear, 3.25 dB. Measured efficiencies are slightly higher than simulated and this is attributed to the lens fiber used that collimates the beam to a 5 μm MFD spot. Using a 3 μm MFD fiber, the measured efficiencies improved respectively to 0.56 dB, 0.84 dB, and 0.95 dB. Use of the smaller MFD fiber resulted in better efficiency since radiation loss to the substrate are not as dominant as they are with a larger MFD fiber. Specifically, the efficiency of the constant-loss taper measured at 0.56 dB is remarkably high given its short 15 μm length.

5. Conclusion

A new design strategy of engineering losses constant through the taper has been introduced using a Lagrangian approach, and an original, constant-loss taper was derived. We showed with 3D-FDTD calculations that the constant-loss taper is both more efficient and robust than the linear and parabolic tapers. Finally, using a short 15-μm-long taper the efficiency of the constant-loss taper was measured at 0.56 dB, the highest efficiency per length ratio ever reported for a nanophotonic taper.

Acknowledgment

This work was funded by the Fonds de Recherche du Québec - Nature et Technologies (FRQNT), the Natural Sciences and Engineering Research Council of Canada (NSERC) and the Canadian Microelectronics Corporation (CMC). Part of the devices' fabrication was accomplished using facilities from the McGill Nanotools Microfab (MNM, McGill University), the Microfabrication Laboratory (LMF, École Polytechnique de Montréal), and the Laboratory of Micro and Nanofabrication (LMN, INRS); the authors acknowledge the staff of these facilities for helping with the fabrication. We also thank Dr. Shurui Wang for help with device testing.